Available online at www.sciencedirect.com
ScienceDirect
Catalysis Today 121 (2007) 237–245
CATALYSIS TODAY
www.elsevier.com/locate/cattod

On the mechanism of model diesel soot-O_2 reaction catalysed by Pt-containing La^{3+}-doped CeO_2 A TAP study with isotopic O_2

A. Bueno-López, K. Krishna, B. van der Linden, G. Mul, J.A. Moulijn, M. Makkee *

Reactor & Catalysis Engineering, DelftChemTech, Delft University of Technology, Julianalaan 136, NL 2628 BL Delft, The Netherlands

Available online 24 August 2006

Abstract

Pt supported on CeO_2 and 10 wt.% La^{3+}-doped CeO_2 catalysts have been prepared, characterised and tested for soot oxidation by O_2 in TGA. The reaction mechanism has been studied in a TAP reactor with labelled O_2. Isotopic oxygen exchange between molecular O_2 and 'O' on the support/catalyst was observed and soot oxidation is being carried out by lattice oxygen. TAP studies further show that Pt improves O_2 adsorption and, therefore, 5 wt.% Pt-containing catalysts are more active for soot oxidation than the counterpart supports. In addition, CeO_2 doping by La^{3+} leads to an improved support, since La^{3+} stabilises the structure of CeO_2 when calcined at high temperature (1000 °C) and minimises sintering. In addition, La^{3+} improves the Ce^{4+}/Ce^{3+} reduction as deduced from H_2-TPR experiments and favours oxygen mobility into the lattice. A synergetic effect of Pt and La^{3+} is observed, Pt-containing La^{3+}-doped CeO_2 being the most active catalyst for soot oxidation by O_2 among the samples studied.

Keywords: Catalysed soot oxidation; Ceria; Lantana; Platinum; Solid solution; Diesel pollution control; Soot; Temporal analysis of products; TAP; Isotopic exchange

1. Introduction

CeO_2-based catalysts are receiving much attention mainly due to their unique properties for automotive exhaust purification [1,2]. Three-way catalysts (TWC) that can eliminate CO, hydrocarbons (HC), and NO_x simultaneously are effective for gasoline-powered engines. These engines operate at near stoichiometric HC/O_2 conditions and this is a prerequisite for proper TWC behaviour. Most TWC formulations combine CeO_2-based materials with noble metals [3]. Doping with trivalent cations into the CeO_2 lattice modifies the physico-chemical properties by creating oxygen vacancies inside the parent oxide [4]. Unfortunately, TWC like systems are not useful for cleaning pollutants in exhaust gas of diesel engines. Harmful compounds emitted by diesel engines are particulate (soot), NO_x, and small amounts of CO and HC [5]. One of the limitations in using a catalytic converter such as TWC in diesel engines is that these engines run under excess O_2 conditions, which is reflected in high levels of O_2 (5–15%) in the exhaust gas. Due to the lean-burn conditions in the diesel engines, NO_x reduction cannot be achieved by reductants in the exhaust gas, and selective catalytic reduction with urea or hydrocarbons as a reductant has been proposed [6,7]. Furthermore, for spontaneous diesel soot oxidation high temperatures are necessary, around 600 °C, much higher than the typical value for diesel exhaust gases. Soot loaded filter regeneration can be carried out by pulsing fuel periodically in the exhaust, whose combustion raises the temperature and ignites the soot collected in the filter. However, fuel penalty is a handicap and run-away phenomena are often encountered which can even melt the filter. Catalytic soot oxidation is an option to improve filters regeneration at low temperatures, and new catalysts are being investigated and developed for this purpose.

In a previous study it has been shown that La^{3+} significantly enhances the catalytic activity of CeO_2 in soot oxidation by O_2 [8] and that the optimum La^{3+} loading has been found about 5–10 wt.%. The incorporation of La^{3+} into the CeO_2 lattice promotes the formation of active oxygen species, the active

* Corresponding author. Tel.: +31 15 278 1391; fax: +31 15 278 5006.
E-mail address: m.makkee@tudelft.nl (M. Makkee).

0920-5861/$ – see front matter © 2006 Elsevier B.V. All rights reserved.
doi:10.1016/j.cattod.2006.06.048

species for soot oxidation mainly due to the increase in BET surface area (from 2 to 20 m^2/g for CeO_2 and 10% La^{3+} doped CeO_2, respectively, both calcined at 723 °C) and the improvement of the redox properties of Ce^{3+}/Ce^{4+} couple. However, La^{3+}-doped CeO_2 catalysts are only active when in *tight contact* with soot. Further studies on the composition of the catalysts have been performed to obtain more active formulations that combine Pt along with different CeO_2-based supports. The objectives of this paper are:

(i) Preparation and characterisation of CeO_2, La^{3+}-doped CeO_2, and Pt supported on the above supports.
(ii) Soot oxidation activity of different supports and Pt-containing catalysts with O_2.
(iii) Elucidation of soot oxidation mechanism in a TAP reactor by studying the interaction of $^{18}O_2$ with the different supports, Pt-containing catalysts and soot–catalyst mixtures.

2. Experimental

2.1. Catalyst preparation

$Ce(NO_3)_3{\cdot}6H_2O$ (Aldrich, 99%), $La(NO_3)_3{\cdot}6H_2O$ (Merck, 99%) and $[Pt(NH_3)_4](NO_3)_2$ (Aldrich, 99.995%) precursors were used. For the preparation of CeO_2, $Ce(NO_3)_3{\cdot}6H_2O$ was calcined in air at 1000 °C for 90 min (heating rate 10 K/min) and for the preparation of 10 wt.% La^{3+}-doped CeO_2 (CeO_2La) the required amounts of $Ce(NO_3)_3{\cdot}6H_2O$ and $La(NO_3)_3{\cdot}6H_2O$ were mixed in a mortar and calcined in similar conditions to those used for CeO_2. CeO_2 and CeO_2La are used to denote the CeO_2 and La^{3+}-doped CeO_2 supports, respectively.

5 wt.% Pt-containing catalysts were prepared by impregnation of 1 g of the respective support with 2 ml of a 0.013 M aqueous $[Pt(NH_3)_4](NO_3)_2$ solution. The obtained mixture was dried at 100 °C followed by platinum precursor decomposition at 500 °C in air for 5 h (heating rate 1 K/min). The actual amounts of platinum on the fresh, calcined, and spent catalysts were not determined. Catalysts are denoted by $PtCeO_2$ and $PtCeO_2La$.

2.2. Catalyst characterisation

The BET surface areas of the supports (before the platinum loading and calcination) were determined by physical adsorption of N_2 at −196 °C in an automatic volumetric system (Autosorb-6, Quantachrome) and the meso- and macroporosity was characterised by Carlo Erba 2000 mercury porosimeter.

Raman spectra were recorded in a Renishaw Raman Imaging Microscope, system 2000 with an Ar laser (514 nm). The Ramascope was calibrated using a silicon wafer.

X-ray diffractograms were recorded in a Philips X-ray diffractometer, PW 1840, with Ni-filtered Cu Kα radiation ($\lambda = 0.15418$ nm).

Temperature programmed reduction by H_2 (H_2-TPR) was carried out in a tubular quartz reactor (inner diameter 5 mm), that was coupled to a TCD detector for monitoring H_2 consumption. Water (from desorption or formed from reaction) was removed by a membrane before entering the TDC-detector. The experiments were conducted by heating the fresh samples (50 mg) at 10 K/min from room temperature to 1000 °C in 30 ml/min flow of 7.7 vol.% H_2 in Ar. CuO was used as calibration reference to quantify the total amount of H_2 consumed during the experiments.

2.3. Catalyst performance

Soot oxidation in O_2 was studied in a thermogravimetric analyser (TGA, Mettler Toledo, TGA/SDTA851[e]). Oxidation experiments consisted of heating soot–catalyst mixtures from 30 to 700 °C at 10 K/min in 100 ml/min flow of 20 vol.% O_2 in He flow. Loose contact mixtures of soot and catalyst (mixed with a spatula) in 1:4 weight ratio were used to carry out the soot oxidation experiments. Experiments were performed with 4 mg of soot-catalyst or soot–support mixtures diluted with SiC to dissipate heat, and approximately 50% of the crucible bottom volume was filled with SiC to avoid gas diffusion effects.

Temporal analysis of products (TAP) was used to analyse the interaction of gas-phase O_2 with catalysts between 200 and 600 °C in the Multitrack set-up using labelled O_2 ($^{18}O_2$, <1% $^{16}O_2$ impurity) and Ar (reference gas). A cylindrical reactor (7 mm i.d.) containing the sample was connected to an ultra-high vacuum system (10^{-6} Pa). Oxygen pulses, typically consisting of $\sim 10^{16}$ molecules of $^{18}O_2$, were fed to the catalyst bed using high-speed gas pulsing valves. The reactor is coupled to three mass spectrometers that are able to measure the components of the gas leaving the reactor with a maximum sampling frequency of 1 MHz. In separate experiments, Ar gas was pulsed through the sample bed at different temperatures to obtain inert gas-interaction profiles, which were used as reference. The experiments were carried out with 100 mg of sample (around 10^{20} molecules of CeO_2) and this amount was much higher than the total amount of gas molecules pulsed. The response was normalised in respect to the Argon pulse and the mass balance of the pulse, if the response of the pulse has a pulse shape, is closed. The gas pulses were introduction 0.1 s after the data acquisition has been started. Around 10^4 pulses would be necessary for complete exchange of lattice oxygen by $^{18}O_2$ ($CeO_2/^{18}O_2$ molar ratio of 1). Therefore, it was assumed that the small number of $^{18}O_2$ pulses used in studying its interaction at each temperature do not change the nature of the supports.

The protocol of the TAP experiments consisted of (i) stabilisation of the temperature at 200 °C in vacuum, followed by $^{18}O_2$ pulsing until no uptake was observed (the steady state was reached within about 125 pulses), (ii) subsequently, the temperature was increased to 300, 400, 500, and 600 °C and $^{18}O_2$ was pulsed at each of these temperatures. Above 200 °C, $^{18}O_2$ uptake was not observed after 25 pulses and it can be assumed that the catalyst is saturated. Similar experiments with 10 mg of soot mixed with 100 mg of the selected supports and catalysts (tight contact, mixed in a mortar) were performed as well.

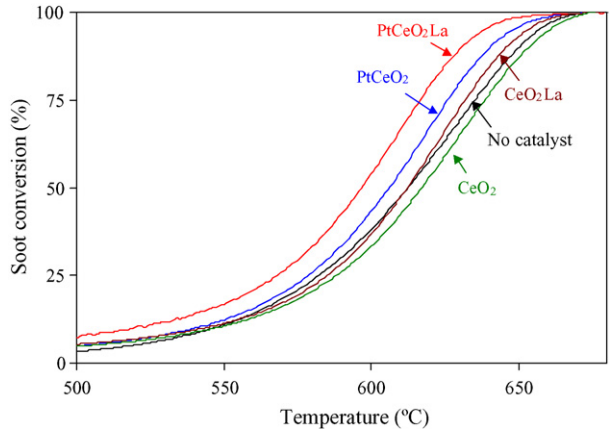

Fig. 1. Soot oxidation by O_2 in TGA in loose contact.

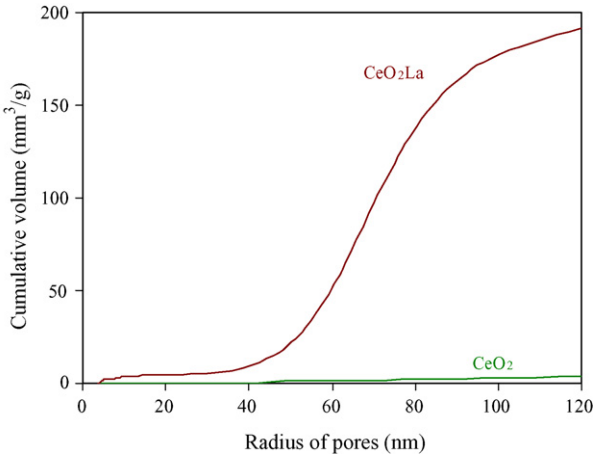

Fig. 2. Cumulative pore volume of supports as determined by Hg porosimetry.

3. Results

3.1. Catalytic soot oxidation activity in TGA

Fig. 1 shows the soot conversion profiles in loose contact with temperature over different supports and Pt-containing catalysts. The supports did not significantly improve soot oxidation within the experimental reproducibility, while the Pt-containing catalysts decreased the soot oxidation temperature to some extent. The activity of the different catalysts and supports follows the trend:

$$PtCeO_2La > PtCeO_2 > CeO_2La > CeO_2 \sim \text{uncatalysed}$$

Pt-containing catalysts were more active than the corresponding supports, and La^{3+}-doping improved the catalytic activity of CeO_2. Therefore, the combination of La^{3+}-doped CeO_2 with Pt ($PtCeO_2La$) yielded most active catalyst among the samples studied.

3.2. Catalyst characterisation

The BET surface area of the CeO_2 and CeO_2La supports (Table 1) were 2 and 20 m^2/g, respectively [4,9]. These BET area values indicated that La^{3+} stabilised CeO_2 and, therefore, the La^{3+}-doped CeO_2 was less affected due to sintering by the high calcination temperature than the undoped CeO_2 support.

Results of the mercury intrusion porosimetry characterisation are depicted in Fig. 2. Hg intrusion measurements show that La^{3+} stabilised the CeO_2 pore structure. The calcination treatment had small influence in CeO_2La if compared with CeO_2. The porosity in the range of mesopores (2–50 nm) and macropores (>50 nm) were negligible in the CeO_2 support while they increase in CeO_2La support.

Table 1
BET surface area and crystallite size of the supports

Support	BET (m^2/g)	Crystallite size[a] (nm)
CeO_2	2	78
CeO_2La	20	30

[a] From XRD.

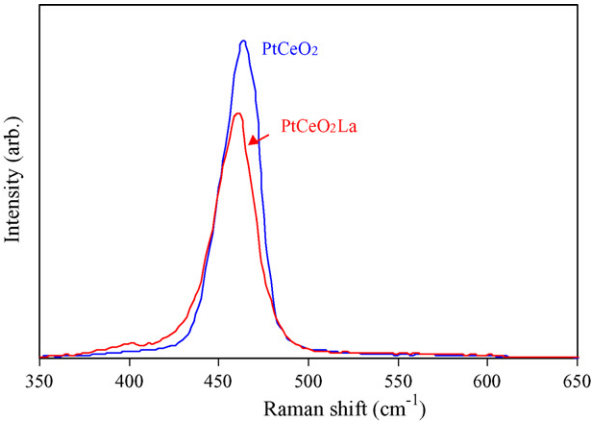

Fig. 3. Raman spectra of catalysts.

Raman spectra of the catalysts are shown in Fig. 3. The band around 460 cm^{-1} observed in both spectra was the only allowed Raman mode (F_{2g}) of the fluorite-type structure [10,11], which is characteristic of CeO_2. The fluorite structure is a face centred cubic structure (fcc), in which the cations are placed in the

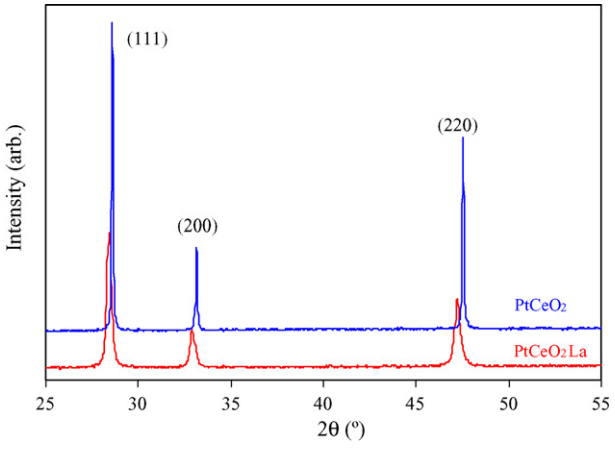

Fig. 4. X-ray difractograms of catalysts.

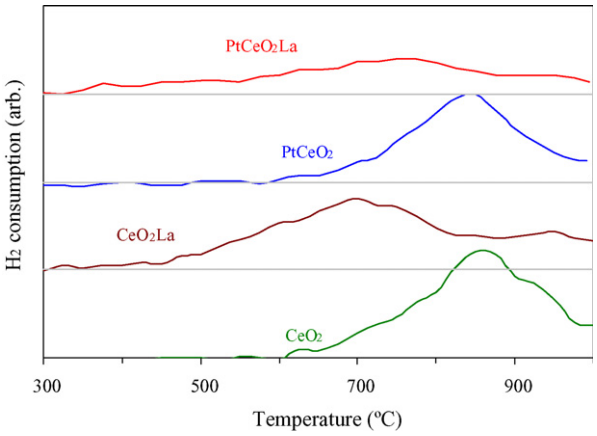

Fig. 5. H_2 consumption profiles during H_2-TPR.

Table 2
H_2 consumption during H_2-TPR

Sample	mmol $H_2/g_{catalyst}$	mol H_2/mol_{Ce}
CeO_2	0.53	0.09
CeO_2La	0.62	0.12
$PtCeO_2$	0.48	0.09
$PtCeO_2La$	0.62	0.12

corners and in the centre of faces and oxygen atoms are located in the tetrahedral sites. The Raman spectra of these fluorite-type oxide structures are dominated by oxygen lattice vibrations and are sensitive to the crystalline symmetry [12]. La^{3+} affected the structure of the support, and the position of the maximum shifted from 465 cm^{-1} for $PtCeO_2$ until 460.2 cm^{-1} for $PtCeO_2La$. From Raman spectra it can be deduced that La^{3+} is located in the CeO_2 lattice. Bands due to La_2O_3 (around 400 cm^{-1}) and oxygen adsorbed on Pt (around 600 cm^{-1}) were observed to some minor extent, but their contribution is not significant.

The X-ray diffractograms of the catalysts are shown in Fig. 4. Both catalysts presented the characteristic peaks of the true mixed-oxide phase with the cubic fluorite-type structure typical of CeO_2 [13]. A shift in the peak position to lower 2θ was observed due to incorporation of larger La^{3+} ion (1.15 Å) into the lattice of CeO_2 (Ce^{4+} 1.01 Å). La_2O_3 and Pt/PtO characteristic peaks were not observed, indicating that most of the La^{3+} was incorporated into the CeO_2 lattice and small Pt crystallite sizes will have a particle size below 10 nm.

From XRD patterns in Fig. 4, the average crystallite size (D) of CeO_2 and La^{3+}-doped CeO_2 were determined using the Scherrer equation

$$D = \frac{K\lambda}{\beta \cos\theta}$$

where λ is the X-ray wavelength, K the particle shape factor, taken as 0.94 [11], β defined as the width at half maximum and θ is the diffraction angle of the respective peak. The average crystallite sizes, reported in the Table 1, are 78 and 30 nm for CeO_2 and CeO_2La, respectively, confirming the resistance of La^{3+}-doped CeO_2 towards sintering in comparison to bare CeO_2.

The redox properties of the different samples were analysed by H_2-TPR. H_2-consumption profiles are shown in Fig. 5 and the total amount of H_2 consumed were quantified and compiled

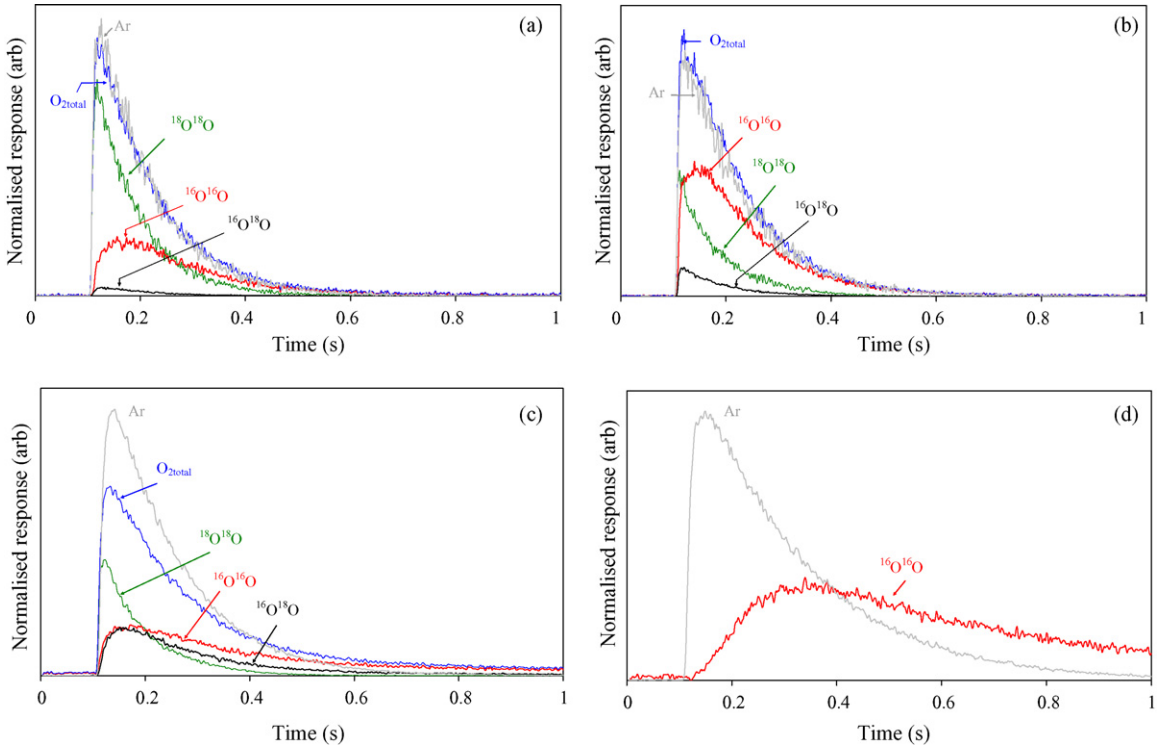

Fig. 6. Pulses of $^{18}O^{18}O$ at 600 °C over (a) CeO_2, (b) CeO_2La, (c) $PtCeO_2$, and (d) $PtCeO_2La$.

in Table 2. It is generally accepted that two peaks characterise the H_2-reduction profile of ceria [14]. A low temperature peak is attributed to the reduction of the surface layers of Ce^{4+} and a high temperature peak is due to the bulk CeO_2 reduction. CeO_2 and $PtCeO_2$ samples did not show the low temperature peak in Fig. 5 due to the extremely low surface area of this support (2 m^2/g). On the contrary, profiles of CeO_2La and $PtCeO_2La$ (support surface area of 20 m^2/g) were different to those of CeO_2 and $PtCeO_2$. The H_2 consumption onset temperature of CeO_2La and $PtCeO_2La$ decreased significantly in comparison to CeO_2 samples, indicating surface Ce^{4+} reduction. However, two peaks were not observed but a broad band due to concurrent surface and bulk reduction [14]. This indicates an improved oxygen mobility in La^{3+}-doped CeO_2 lattice, that La^{3+} is influencing the CeO_2 redox properties. An additional improvement in low temperature H_2-consumption is observed in $PtCeO_2La$ in comparison to CeO_2La. This can be explained by the ability of Pt to activate H_2, allowing spill-over of hydrogen [15].

Comparison of the amounts of H_2 consumed by CeO_2 and CeO_2La (see Table 2) points out that La^{3+} increased the amount of Ce^{4+} that can be reduced by H_2. However, $PtCeO_2La$ and CeO_2La showed similar values, indicating that Pt improved H_2 activation, lowering the reduction temperature, but not the amount Ce^{4+} that can be reduced.

3.3. Catalyst–O_2 interaction by TAP

The interaction of O_2 with the catalysts and supports was investigated in a TAP reactor. The responses of the species leaving the reactor after pulses of labelled O_2 ($^{18}O^{18}O$) at 600 °C are shown in Fig. 6. At 600 °C, all samples tested retained part or all the $^{18}O^{18}O$ pulsed and oxygen from the lattice (^{16}O) released as $^{16}O^{18}O$ and/or $^{16}O^{16}O$. Fig. 6a and b comparison pointed out that La^{3+} increased the amount of oxygen exchanged, and comparison between Fig. 6a and c indicated that Pt further enhanced oxygen exchange. A synergetic effect of La^{3+} and Pt was observed in Fig. 6d. All the $^{18}O^{18}O$ pulsed was retained on the sample and only $^{16}O^{16}O$ was released.

Some information was obtained comparing the shape of the $O_{2\ total}$ profiles ($O_{2\ total}$ = $^{16}O^{16}O$ + $^{16}O^{18}O$ + $^{18}O^{18}O$) and Ar profiles, considered as reference. $O_{2\ total}$ profiles in Fig. 6a and b (samples without Pt) were similar to Ar profiles, which indicated that the exchange of oxygen occurred very rapid and the oxygen uptake rate was similar to the oxygen release rate. On the contrary, in Fig. 6c and d, $O_{2\ total}$ shapes were different to Ar profiles, and $O_{2\ total}$ were delayed in comparison to Ar. This indicated that the oxygen uptake rate was faster than the oxygen release rate, which pointed out that Pt was playing a role in the capture of $^{18}O^{18}O$, improving the rate of this process. These results evidenced that the extent of the oxygen exchange depended on the $^{18}O^{18}O$ uptake rate, which was improved by Pt, and also depended on the oxygen storage capacity of the rare earth framework, which was improved by La^{3+}.

The percentages of the different species leaving the reactor in the experiments performed at different temperatures between 200 and 600 °C were quantified from profiles as those shown in Fig. 6. Fig. 7 features these percentages as a function of

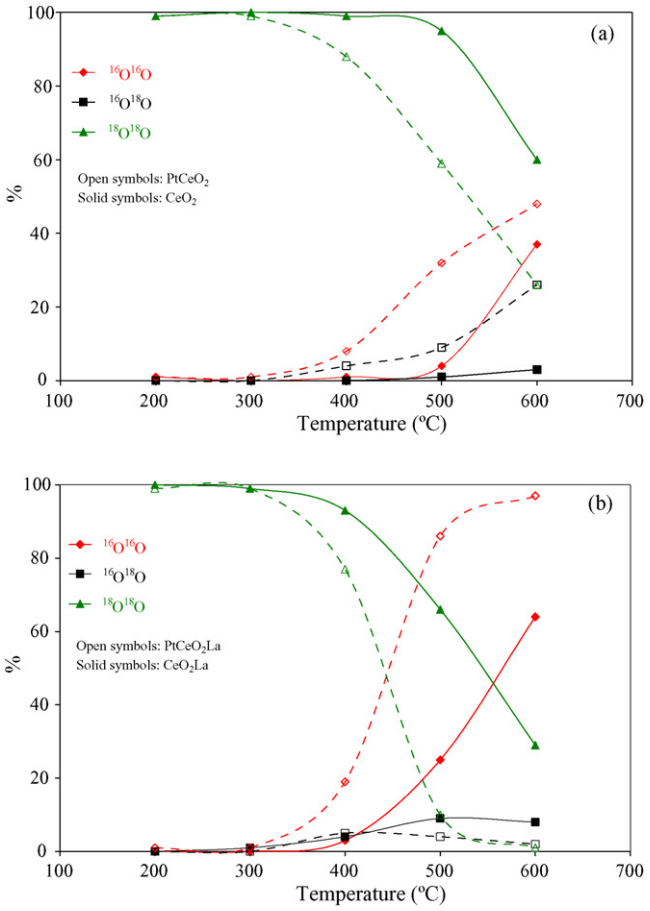

Fig. 7. Percentage of the different O_2 species evolved after pulses of ^{18}O–^{18}O at different temperatures over (a) CeO_2 and $PtCeO_2$, and (b) CeO_2La and $PtCeO_2La$.

temperature. The oxygen exchange process in CeO_2 hardly occurred below 600 °C, and at 600 °C, part of the $^{18}O^{18}O$ pulsed was captured and mainly $^{16}O^{16}O$ was released (Fig. 7a). Pt decreased the oxygen exchange onset temperature and increased the extent of isotopic exchange, attributed to the improvement of the $^{18}O^{18}O$ uptake rate (compare $PtCeO_2$ and CeO_2 in Fig. 7a). The formation of $^{16}O^{18}O$ along with $^{16}O^{16}O$ at high temperatures is an evidence for the change in the exchange mechanism due to Pt. La^{3+} also decreased the oxygen exchange onset temperature and improved the extent of the exchange (compare CeO_2 in Fig. 7a with CeO_2La in Fig. 7b), due to the modification of the oxygen storage capacity of the CeO_2 framework, and the synergetic effect between La^{+3} and Pt was also observed (Fig. 7b).

The interaction of $^{18}O_2$ with soot–catalyst mixtures at 600 °C is shown in Fig. 8. From the interaction profiles it can be concluded that, insignificant $^{18}O_2$ was exchanged with soot even at 600 °C (very small concentration of $C^{18}O$ was released as a result of the direct gas-phase oxidation of $^{18}O_2$ with soot). As expected, all the catalysts improved soot oxidation and, whatever the catalyst, all the $^{18}O^{18}O$ pulsed was consumed at 600 °C and ^{16}O-containing soot oxidation products were observed. This indicated that the $^{18}O^{18}O$ pulsed sticks on the catalysts and ^{16}O from the lattice reacted

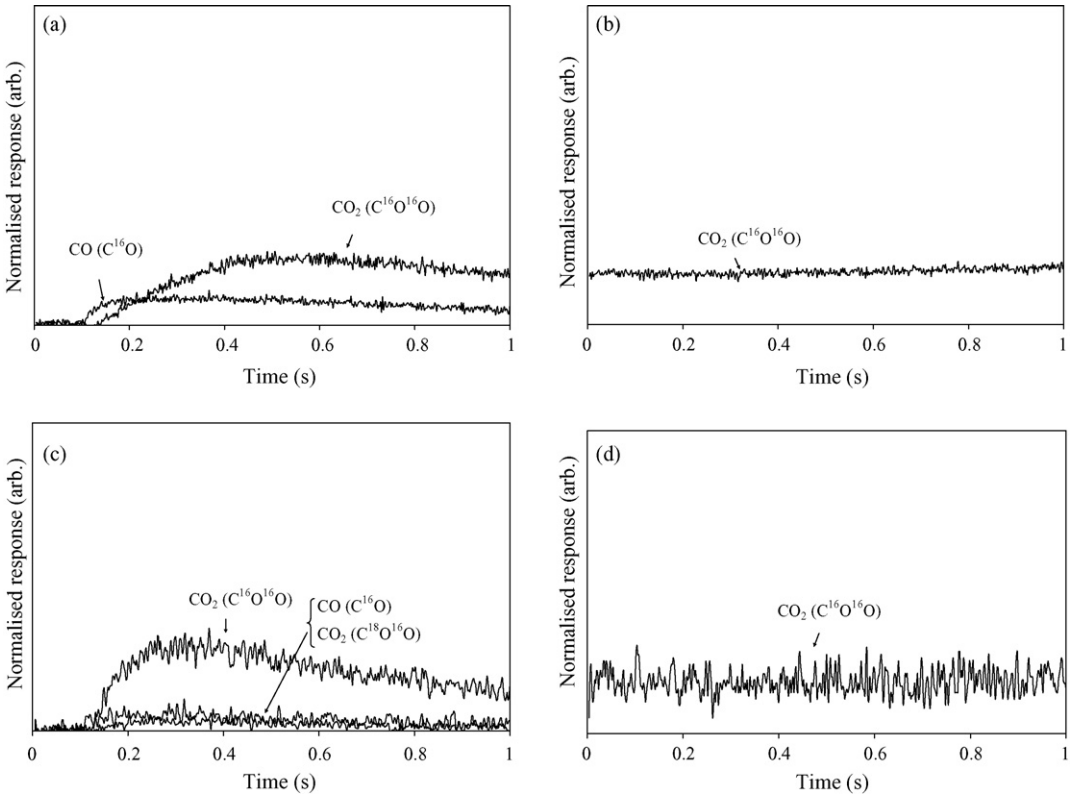

Fig. 8. Pulses of $^{18}O^{18}O$ at 600 °C over soot–catalyst mixtures: (a) CeO_2, (b) CeO_2La, (c) $PtCeO_2$, and (d) $PtCeO_2La$.

with soot. The differences between the CeO_2 (Fig. 8a and c) and CeO_2La containing samples (Fig. 8b and d) had to be noted. In CeO_2 containing samples, $C^{16}O$, $C^{18}O^{16}O$ and/or $C^{16}O^{16}O$ released after $^{18}O^{18}O$ was pulsed, and very broad bands were observed. This indicated that $^{18}O^{18}O$ uptake rate was much faster than sequential reactions. On the contrary, the CO_2 profiles corresponding to La^{3+}-containing catalysts did not show any shape and a continuous CO_2 release occurred (even without $^{18}O^{18}O$ pulsing). These differences pointed out that in La^{3+}-free catalysts, $^{18}O^{18}O$ pulse was the driving force for soot oxidation, while in La^{3+}-containing catalysts the oxygen in the lattice itself oxidised soot and the $^{18}O^{18}O$ pulsed filled the vacant sites created due to soot oxidation. This important difference should be attributed to the improvement of the oxygen storage capacity and redox properties originated by La^{3+} in the CeO_2 lattice.

4. Discussion

As observed from BET surface area, mercury intrusion pore size distribution, XRD and Raman, doping CeO_2 with La^{3+} stabilised pore structure, and the effect of the calcination had more pronounced effect on CeO_2 support. Therefore, the contact area between catalyst and soot is enhanced in the presence of the La-doped materials. At these low surface area the soot oxidation rate in tight contact is closely related to the contact surface area. Furthermore, the collapse of the CeO_2 pore structure affected its redox properties, which was observed in H_2-TPR experiments (Fig. 5). For these two reasons, CeO_2La was more suitable than CeO_2 as Pt support for catalysed soot oxidation.

The participation of lattice oxygen in the catalysed soot oxidation has been demonstrated, and exchange of oxygen between gas phase and CeO_2/CeO_2La lattices was observed (Fig. 8). From TAP data, the following reactions are feasible, which were schematically shown in Figs. 9 and 10.

$$n\mathrm{Ce^{16}O_2} + {}^{18}\mathrm{O^{18}O} \rightarrow (n-1)\mathrm{Ce^{16}O_2}{-}\mathrm{Ce^{18}O_2} + {}^{16}\mathrm{O^{16}O} \quad (1)$$

$$n\mathrm{Ce^{16}O_2}{+}{}^{18}\mathrm{O^{18}O} \rightarrow (n-\tfrac{1}{2})\mathrm{Ce^{16}O_2}{-}\mathrm{Ce^{16}O^{18}O}{+}{}^{16}\mathrm{O^{18}O} \quad (2)$$

$$(n-\tfrac{1}{2})\mathrm{Ce^{16}O_2}{-}\mathrm{Ce^{16}O^{18}O}{+}{}^{16}\mathrm{O^{18}O} \rightarrow (n-1)\mathrm{Ce^{16}O_2}{-}\mathrm{Ce^{18}O_2}{+}{}^{16}\mathrm{O^{16}O} \quad (3)$$

$Ce^{16}O_2$ represents the CeO_2 and CeO_2La supports containing ^{16}O. 'n' indicates the number of $Ce^{16}O_2$ entities, which are much higher than 1 (10^4). In Pt-free samples, $^{18}O^{18}O$ interacts with active sites on the CeO_2 and CeO_2La framework. La^{3+} increased the number of active sites suitable for O_2 adsorption, which is in agreement with the improved oxygen exchange over CeO_2La with regard to CeO_2. $^{18}O^{18}O$ exchange may occur via reaction (1) (both ^{18}O are exchanged) or via reaction (2) (only one of the ^{18}O of the O_2 molecule is exchanged). Formation of $^{16}O^{18}O$ requires adsorption via reaction (2) while $^{16}O^{16}O$ could occur via reaction (1) or by further exchange of the $^{16}O^{18}O$ generated in reaction (2) via reaction (3). At all temperatures, these reactions occurred very rapidly and delay of the $O_{2\ \mathrm{total}}$ profiles with regard to Ar was not observed. Reactions (1)–(3)

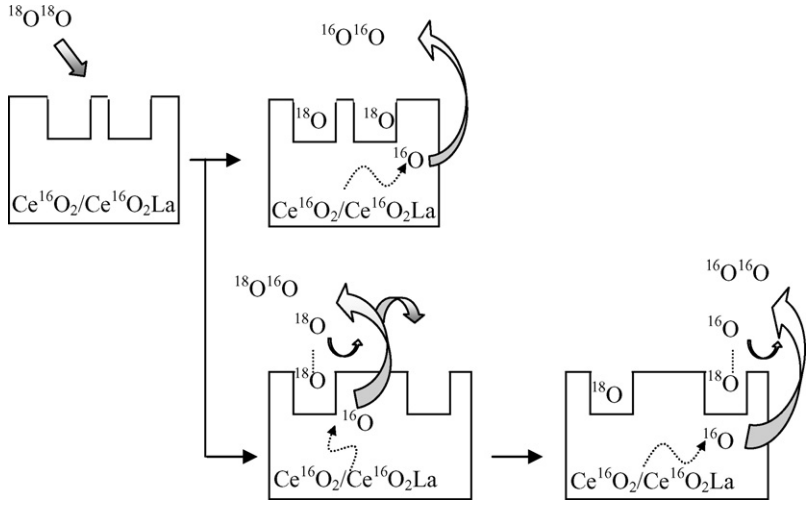

Fig. 9. Interaction of $^{18}O^{18}O$ with CeO_2 and CeO_2La.

are commonly known in the open literature as R^0, R^1, and R^2 exchange mechanisms for the isotopic exchange reaction of oxygen with metal oxides [16].

Although reactions (1)–(3) could potentially occur also over $PtCeO_2$ and $PtCeO_2La$, in this case, the following processes are expected to mainly take place:

$$Pt + {}^{18}O{-}{}^{18}O \rightarrow Pt{-}{}^{18}O^{18}O \quad (4)$$

$$Pt{-}{}^{18}O^{18}O + nCe^{16}O_2 \rightarrow Pt + (n-1)Ce^{16}O_2 - Ce^{18}O_2 + {}^{16}O^{16}O \quad (5)$$

$$Pt{-}{}^{18}O^{18}O + nCe^{16}O_2 \rightarrow Pt + (n-\tfrac{1}{2})Ce^{16}O_2 - Ce^{16}O^{18}O + {}^{16}O^{18}O \quad (6)$$

$$Pt + {}^{16}O{-}{}^{18}O \rightarrow Pt{-}{}^{16}O^{18}O \quad (7)$$

$$Pt{-}{}^{16}O^{18}O + (n-\tfrac{1}{2})Ce^{16}O_2 - Ce^{16}O^{18}O \rightarrow Pt + (n-1)Ce^{16}O_2 - Ce^{18}O_2 + {}^{16}O{-}{}^{16}O \quad (8)$$

In Pt-containing catalysts, the adsorption of $^{18}O^{18}O$ seems mainly to occur on active sites of the noble metal (reaction (4)), which is supported by the fact that Pt strongly increased the $^{18}O^{18}O$ uptake rate. Further transfer of $^{18}O^{18}O$ from Pt to active sites on the CeO_2 or CeO_2La frameworks may occur in a single step (reaction (5)) or throughout the reactions (6)–(8) route. In the presence of Pt, the adsorption rate (reaction (4)) is higher than rates of the additional reaction steps, and the $O_{2\ total}$ curves appeared delayed with regard to Ar. Note that the sequential in $PtCeO_2La$ was much more important than that in $PtCeO_2$, as the amount of O_2 exchanged was also larger. The formation of $^{16}O^{18}O$ over $PtCeO_2$ occurred via reaction (6). As few active sites are available on CeO_2, further conversion of $^{16}O^{18}O$ to $^{16}O^{18}O$ via reactions (6) and (7) was not fully accomplished. On the contrary, a number of active sites were available in CeO_2La and $^{16}O^{18}O$ was hardly detected over $PtCeO_2La$.

In additional TAP experiments (not shown) the exchange rate of $C^{18}O_2$ with all investigated catalysts at all examined temperatures was small in comparison with the rate of

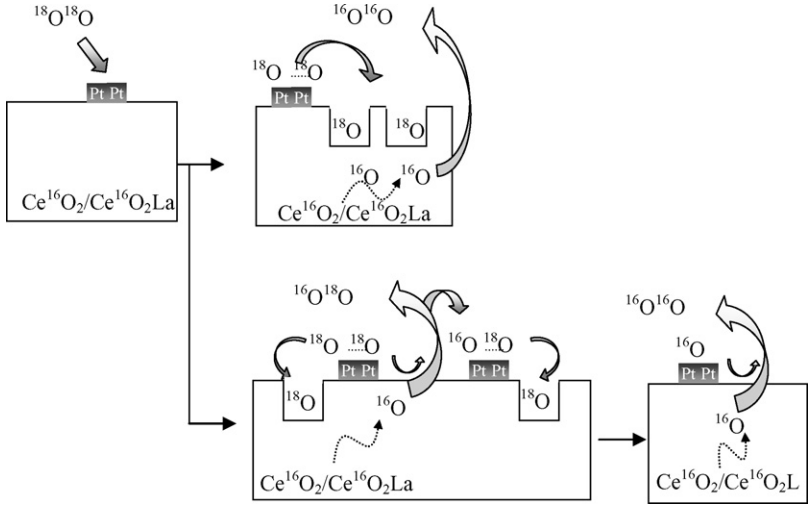

Fig. 10. Interaction of $^{18}O^{18}O$ with $PtCeO_2$ and $PtCeO_2La$.

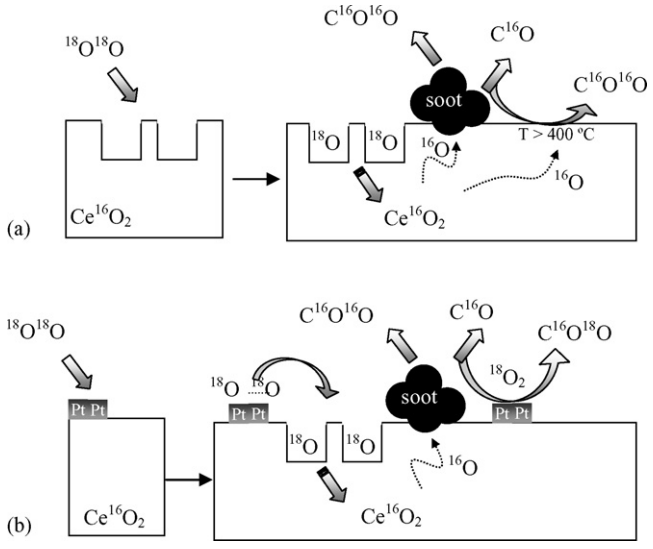

Fig. 11. Soot oxidation mechanism catalysed by: (a) CeO_2 and (b) $PtCeO_2$.

formation of $C^{16}O_2$ and $C^{16}O^{18}O$ (from $C^{16}O$ + dissociated ^{18}O). In other words the exchange of the formed $C^{18}O_2$ with the ^{16}O surface species will play only a minor role in the catalytic soot oxidation mechanism.

From the TAP experiments of O_2 interaction with soot–catalyst, the catalysed soot oxidation mechanisms can be summarised schematically as shown in Figs. 11 and 12. First step of the soot oxidation mechanism catalysed by CeO_2 and $PtCeO_2$ was the adsorption of $^{18}O^{18}O$ on active sites of CeO_2 (reaction (1)) and Pt (reaction (4)), respectively. In $PtCeO_2$, after adsorption, ^{18}O is transferred from Pt to CeO_2 sites through reaction (5) or (6). The O_2 contribution with soot alone is negligible. After $^{18}O^{18}O$ adsorption on the catalysts, the active oxygen species generated on the support (^{16}O) react with soot to yield $C^{16}O$ and $C^{16}O^{16}O$. Note that $^{16}O^{18}O$ and $^{16}O^{16}O$ were not observed in any experiment performed with soot, indicating that the active oxygen species generated on the catalysts did not desorb but reacted with soot. In the La^{3+}-containing samples, the direct oxidation of soot by lattice oxygen seems to be the first step and $^{18}O^{18}O$ fills the vacant sites created on the lattice afterwards, and it is expected that Pt improves the $^{18}O^{18}O$ uptake rate.

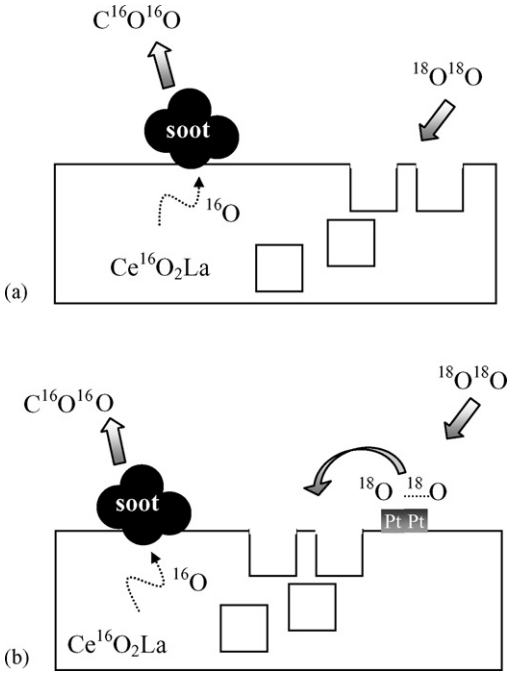

Fig. 12. Soot oxidation mechanism catalysed by (a) CeO_2La and (b) $PtCeO_2La$.

5. Conclusions

The main conclusions of this study are:

- CeO_2La was more suitable than CeO_2 as Pt support due to the thermal stability originated by La^{3+}, also improving the redox properties of the support. Therefore, the combination of La^{3+}-doped CeO_2 with Pt yielded best formulation among those studied.
- Pt-containing catalysts were more active than the corresponding supports for soot oxidation by O_2, and the role of Pt is to increase the O_2 uptake rate on the catalyst.
- Whatever the catalyst, exchange of oxygen between gas phase and CeO_2/CeO_2La lattices was observed in TAP experiments, and soot oxidation was carried out by lattice oxygen but not due to direct reaction between O_2 and soot.
- In La^{3+}-free catalysts, both with and without Pt, soot oxidation under the TAP conditions used only occurred after pulse of O_2, which is the driving force, while, in the La^{3+}-containing catalysts the direct oxidation of soot by lattice oxygen seems to be the first step and gas-phase O_2 fills the vacant sites created on the lattice afterwards.

Acknowledgements

The authors want to thank the Spanish MEC for the fellowship of ABL and Engelhard Corporation for their financial support.

Reference

[1] E.E. Miro, F. Ravelli, M.A. Ulla, L.M. Cornaglia, C.A. Querini, Catal. Today 53 (1999) 631.
[2] J. Kaspar, P. Fornasiero, M. Graziani, Catal. Today 50 (1999) 285.
[3] H.S. Gandhi, G.W. Graham, R.W. Mccabe, J. Catal. 216 (2003) 433.
[4] P. Vidmar, P. Fornasiero, J. Kaspar, G. Gubitosa, M. Graziani, J. Catal. 171 (1997) 160.
[5] J.P.A. Neeft, M. Makkee, J.A. Moulijn, Fuel Process. Technol. 47 (1996) 1.
[6] B.A.A.L. van Setten, M. Makkee, J.A. Moulijn, Catal. Rev. Sci. Eng. 43 (2001) 489.
[7] A. Bueno-Lopez, D. Lozano-Castello, I. Such-Basanez, J.M. Garcia-Cortes, M.J. Illan-Gomez, C.S.M. de Lecea, Appl. Catal. B 58 (2005) 1.
[8] A. Bueno-Lopez, K. Krishna, M. Makkee, J.A. Moulijn, J. Catal. 230 (2005) 237.
[9] A. Bueno-Lopez, K. Krishna, M. Makkee, J.A. Moulijn, Catal. Lett. 99 (2005) 203.
[10] A. Mineshige, T. Taji, Y. Muroi, M. Kobune, S. Fujii, N. Nishi, M. Inaba, Z. Ogumi, Solid State Ionics 135 (2000) 481.

[11] L.N. Ikryannikova, A.A. Aksenov, G.L. Markaryan, G.P. Murav'eva, B.G. Kostyuk, A.N. Kharlanov, E.V. Lunina, Appl. Catal. A 210 (2001) 225.
[12] M. Fernandez-Garcia, A. Martinez-Arias, A. Iglesias-Juez, C. Belver, A.B. Hungria, J.C. Conesa, J. Soria, J. Catal. 194 (2000) 385.
[13] D. Terribile, A. Trovarelli, J. Llorca, C. de Leitenburg, G. Dolcetti, Catal. Today 43 (1998) 79.
[14] G.L. Markaryan, L.N. Ikryannikova, G.P. Muravieva, A.O. Turakulova, B.G. Kostyuk, E.V. Lunina, V.V. Lunin, E. Zhilinskaya, A. Aboukais, Colloids Surf. A 151 (1999) 435.
[15] P. Fornasiero, J. Kaspar, T. Montini, M. Graziani, V. Dal Santo, R. Psaro, S. Recchia, J. Mol. Catal. A 204 (2003) 683.
[16] C. Doornkamp, M. Clement, V. Ponec, J. Catal. 182 (1999) 390.